ELSEVIER

Contents lists available at ScienceDirect

## Remote Sensing of Environment

journal homepage: www.elsevier.com/locate/rse





# Dynamic emergent leaf area in tidal wetlands: Implications for satellite-derived regional and global blue carbon estimates

Peter A. Hawman a, , Deepak R. Mishra , Jessica L. O'Connell

- \* Department of Geography, University of Georgia, Athens, GA 30602-3636, United States
- b Department of Marine Science, Marine Science Institute, University of Texas at Austin, Port Aransas, TX 78373-5015, United States

#### ARTICLE INFO

Edited by Dr. Marie Weiss

Keyword:
Blue carbon
Salt marshes
Tidal wetlands
Leaf area
Carbon modeling
Remote sensing

#### ABSTRACT

The IPCC Special Report on the Ocean and Cryosphere in a Changing Climate highlights the importance of blue carbon in tidal wetlands in combating climate change. In this study, we highlight the uncertainty associated with leaf area index (LAI) estimations in tidal wetlands, specifically salt marshes, a key vegetation parameter for productivity models and Earth System Models (ESM). LAI, derived from satellite reflectance data, is linked to atmospheric carbon exchange and gross primary production (GPP) across vegetative ecosystems. However, estimating salt marsh LAI is challenging because canopy height and density vary across short distances, and tidal flooding alters the atmosphere-exposed leaf area, hereafter called emergent leaf area index (ELAI), at short time scales. Further, in tidal wetlands dominated by species such as Spartina alterniflora, canopy height and density vary across short distances. We present a novel approach for measuring spatiotemporal dynamics in tidal wetland ELAI. We modeled ELAI from vertical LAI profiles and created spatial estimates across tidal periods. We then linked ELAI with eddy covariance carbon (C) fluxes through footprint modeling and revealed correlations between emergent leaf area and C fluxes. Next, we demonstrated that ELAI can be readily estimated across 10-m spatial scales using Sentinel-2 satellite data, even during high tides ( $R^2 = 0.89$ ; NRMSE = 10%). Finally, we showed a common product, MODIS MYD15A2H, underestimated (20%) LAI during dry conditions but overestimated (7-93%) during high flooding. Dynamic ELAI could reduce uncertainties in satellite-derived global GPP products when developing blue carbon budgets for ecosystems threatened by accelerated sea level rise.

### 1. Introduction

Tidal salt marshes are coastal wetlands that constitute a large portion of global blue carbon ecosystems and play an important role in the global carbon cycle (Nellemann and Corcoran, 2009). Frequent tidal flooding transports nutrients, flushes metabolic toxins, and deposits sediment for marsh accretion, which enables tidal wetlands to store 20–25% of the world's soil organic carbon stock, while covering only 4–6% of the world's land area (Yu et al., 2012). While, at short time-scales, tidal flooding submerges plants and reduces atmospheric carbon (C) assimilation (Kathilankal et al., 2008), this reduction is small relative to annual budgets (Forbrich and Giblin, 2015). However, the benefits of tidal flooding can become deficits when flooding is deep or prolonged, resulting in anoxic conditions and reduced soils that diminish nutrient uptake (Mendelssohn and Morris, 2002) causing plant death, channel collapse, and marsh drowning (Crosby et al., 2016; Mariotti, 2020; Smith and Lee, 2015; Voss et al., 2013). As sea-level rise

accelerates, the conservation of marsh ecosystem benefits is uncertain (IPCC, 2019; Schuerch et al., 2018) and depends on both their ability to accrete vertically as a consequence of sediment supply and elevation capital (Langston et al., 2021), and the available space for landward migration (Kirwan et al., 2016). Tidal salt marsh canopies are expected to be inundated more frequently with increasing sea levels, resulting in shifts in vegetation dynamics (Langston et al., 2020) and atmospheric C assimilation. Therefore, it is vital that we understand the nature of leaf area in tidal salt marshes to better model C dynamics and assess marsh vulnerability to climate change. In this study, we present a solution for modeling canopy leaf area exposed to the atmosphere during flooding, here known as emergent leaf area, and link it to atmospheric C assimilation. Our efforts aim to better inform large-scale productivity and Earth system models (ESM), which rely on accurate leaf area estimations

Canopy leaf area, the area over which chlorophyll, photosynthetic and other leaf physiological reactions are arrayed, helps determine

<sup>\*</sup> Corresponding author at: University of Georgia, Department of Geography, 210 Field Street, Athens, GA 30602, United States. E-mail address: pete36@uga.edu (P.A. Hawman).

atmospheric gas exchange during photosynthesis (Nobel, 1983) and is an important component to quantify gross primary production (GPP) (Guo et al., 2009), ecosystem phenology (Running and Hunt, 1993), and responses to climate change (Cleland et al., 2007). Leaf area is a key variable in vegetation productivity and land-surface models (Cowling and Field, 2003) and an important input for ESMs (Park and Jeong, 2021). Leaf area index (LAI), the one-sided leaf area per unit ground area (m² m²), is the common metric for quantifying leaf area and is often used in GPP models (Running et al., 1999). LAI is estimated through satellite remote sensing vegetation indices (Boresjoe Bronge, 2004; Huete et al., 2002; Xie et al., 2019).

Tidal salt marsh leaf area, and wetland leaf area in general, is spatially and temporally dynamic, but not well studied (Asner et al., 2003). Canopy density and height vary across the salt marsh surface due to interactions between nutrient availability, elevation, salinity, and tidal flooding (Chaisson et al., 2022; Mendelssohn and Morris, 2002; Pennings et al., 2005). In tidal salt marshes, where vegetation is often dominated by monocultures of habitat specialists such as Spartina alterniflora, environmental gradients create distinct zones (Pennings et al., 2005). For S. alterniflora marshes, low elevation edges adjacent to water bodies can have frequent and moderate flooding that flushes soils, resulting in high nutrient availability, lower salinity, higher soil oxygen, and taller canopies ( 1 m). In higher elevation mid-marsh to interior areas, canopy heights become shorter ( 1 m) due to physiological stresses related to temperature, high evapotranspiration, salinity, and redox potential (Mendelssohn and Morris, 2002). In addition to the spatial heterogeneity of canopy structure, frequent tidal flooding changes the amount of emergent leaf area exposed to the atmosphere and available for C exchange at various timescales (hours to months). Further, patterns in canopy structure can shift if flooding becomes prolonged and stagnate, for example, when sea level rise overwhelms vertical accretion. Deep prolonged flooding deprives plants of oxygen and results in plant death. Thus, even small changes in elevation (0.1 m) can result in differences in plant morphology and dynamics across both space and time.

The transient nature of tidal waters on the marsh surface also poses challenges for remote sensing studies aimed at productivity modeling, a common method to estimate blue carbon storage regionally and globally (Feagin et al., 2020; Najjar et al., 2018). Tidal flooding alters the reflectance characteristics of submerged and partially submerged vegetation (Cho et al., 2008; Kearney et al., 2009; Mishra and Ghosh, 2015), resulting in noisy time-series data (Narron et al., 2022; O Connell et al., 2017). This causes uncertainty in productivity estimates (Feagin et al., 2020; Tao et al., 2018) and aboveground biomass modeling (Kearney et al., 2009). Studies often flag and remove tidally impacted data (Dechant et al., 2022; Sun et al., 2021; Tao et al., 2018), find nonsignificant impacts (Feagin et al., 2020), or do not account for flooding in their analyses (Ge et al., 2016; Kang et al., 2018; Wu et al., 2015; Yan et al., 2008, 2010). Moderate resolution LAI products, such as NASA s MODIS LAI 8-day product (MYD15A2H) (Myneni et al., 2015), are not parameterized for wetlands but are frequently used in carbon studies assuming dry substrate conditions during satellite overpass (Kang et al., 2018; Wu et al., 2015, p. 201; Yan et al., 2010). The resulting uncertainties in LAI estimations, therefore, have the potential to propagate through productivity models and ESMs (Park and Jeong, 2021).

Dynamic emergent leaf area, i.e., highly variable leaf area caused by frequent tidal flooding, poses challenges to modeling C fluxes. Through the Eddy Covariance (EC) method, which measures surface-atmosphere CO<sub>2</sub> fluxes, past studies have observed the suppression of C assimilation during tidal flooding (Forbrich and Giblin, 2015; Kathilankal et al., 2008; Moffett et al., 2010; Nahrawi et al., 2020). However, the reported reductions varied depending on species and hydrology, and this variation can impact broader assessments of coastal wetland productivity (Feagin et al., 2020; Tao et al., 2018) and blue carbon estimates (Chapin et al., 2006; Nellemann and Corcoran, 2009; Troxler et al., 2013). So far,

the link between emergent leaf area and atmospheric C fluxes has not been made and understanding it could provide insight into ecosystem carbon budgets, particularly related to impacts surface waters have on C fluxes (Cai et al., 1999).

In this study, we used in situ LAI measurements collected in a S. alterniflora tidal salt marsh within the Georgia Coastal Ecosystems Long Term Ecological Research (GCE-LTER) site located on Sapelo Island, Georgia, USA. We used canopy LAI vertical profiles to model emergent LAI (ELAI), capturing tidal flooding across the marsh surface, and linked it through EC flux tower footprint predictions (FFP) (Kljun et al., 2015), representing the C flux source areas, to measured net ecosystem exchange (NEE). We then scaled ELAI estimations to 10-m Sentinel-2 surface reflectance data (5-day returns) to show that emergent leaf area could be modeled from satellite data at the needed spatial and temporal scale using reflectance only. Finally, we compared ELAI estimations to the commonly used MODIS 500-m 8-day LAI product (MYD15A2H) to highlight uncertainties in LAI products for tidal wetlands. To our knowledge, this is the first time emergent LAI has been measured and estimated for salt marshes, which may have significant implications for future regional blue carbon studies that rely on satellite

### 2. Materials and methods

### 2.1. Study area

We conducted our study in the Georgia Coastal Ecosystems Long Term Ecological Research (GCE-LTER) site located on Sapelo Island, Georgia, USA (Fig. 1). Tidal salt marshes there were dominated by *S. alterniflora* and experienced semi-diurnal flooding with average tidal ranges of approximately 1.2 m. *S. alterniflora* canopy heights typically ranged from 0.5 to 1.0 m (Hladik et al., 2013) with minimum and maximum canopy heights of 0.3 and 1.6 m, respectively. Most of the marsh canopies were considered mid-marsh and interior areas with canopies 0.6 m in height (Fig. 1c). Salinity levels in the adjacent tidal river averaged 25.68 ppt (sd 4.57). Mean marsh platform elevations around the sampling locations were 0.71 (sd 0.2) m NAVD 88. Further information on study location and climate characteristics can be found in Hawman et al. (2021).

### 2.2. In situ vegetation sampling

Our first objective was to measure in situ leaf area within our study site, its variation across marsh zones (edge, mid-marsh, and interior), and its vertical profile through the canopy height to determine the amount of ELAI under varying water levels. We measured leaf area index monthly for 5 months (June October 2021) via a ceptometer (AccuPAR LP-80, Decagon Devices, Inc., Pullman, WA, USA) at 18 permanent 1-m<sup>2</sup> vegetation plots located approximately 650 m north of the GCE-LTER flux tower (Fig. 1c). Plots represented three *S. alterniflora* canopy types across an elevation gradient (short plants in the marsh interior: at a modium height plants in the mid marsh; n. 6, and taller plants at

6, medium height plants in the mid-marsh: n 6, and taller plants at the marsh edges: n 6). We measured LAI at intervals of 10 cm (interior and mid-marsh) and 20 cm (marsh edges) through the canopy height at each plot (Ramsey et al., 2004).

Stem heights and stem densities were measured once a month for each vegetation plot (Pennings, 2022). Stem heights for all stems within a quadrat (interior & mid-marsh: 0.25 0.25 m; marsh edges: 0.5 0.5 m) were measured to the nearest 1 cm and stems were counted. Quadrat size was increased at the marsh edge where stems are not as dense to sample representative areas. We then approximated stem densities to a meter squared area by dividing the number of stems measured within the quadrat by the quadrat area.

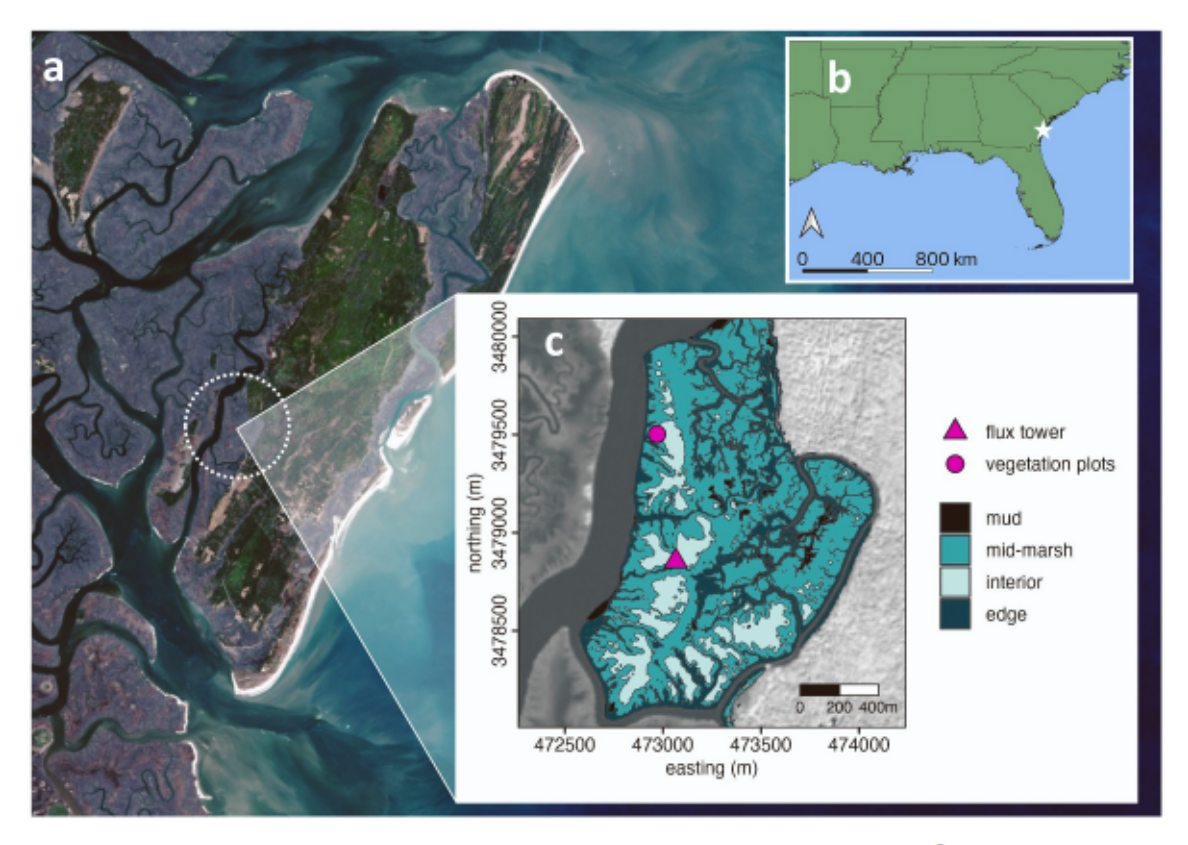


Fig. 1. a) Sapelo Island, Georgia on the b) eastern United States Atlantic Coast. c) Map showing the locations of the GCE-LTER flux tower and the vegetation plots. Colored areas show the Sparting alterniflora marsh zones (Hladik et al., 2013). Background images are a) Landsat 8 and c) Sentinel-2.

### 2.3. Canopy LAI profile modeling

To estimate BLAI for each marsh zone at a given water level and understand the distribution of LAI within the canopy profile, we used non-linear regression to fit models that describe the cumulative LAI with canopy height. We oriented our profiles beginning at the top of canopy and progressing downward. We did so to approximate the amount of LAI above a given height within canopy, mimicking the emergent leaf area during tidal flooding. We tested log-based sigmoidal functions, such as the Weibull cumulative distribution function (Weibull, 1951), as their shape closely approximates the LAI canopy profiles and has been used successfully in forest canopy modeling (Teske and Thistle, 2004; Yang et al., 1993).

Log-based sigmoidal functions have 4 parameters describing the upper limit (c), lower limit (d), slope (b), and inflection point (e) of the curves. The Weibull Type-1 function has an asymmetric inflection point parameter (e), allowing the function to accommodate an asymmetric curve (Christensen and Nyholm, 1984):

$$LAI = c + (d - c)exp(-exp(b(log(h_k) - log(e))))$$
(1)

where  $h_X$  is the height within the canopy and b, c, d, and e are fitted parameters representing the slope, upper limit, lower limit, and midpoint. In the 3-parameter form of the Weibull Type-1 function, we set the upper limit (c) to 0 since LAI is 0 above the canopy.

We also tested linear regression models (linear, quadratic, and cubic). Regression analysis of log-based sigmoidal functions was conducted using the dre package (Ritz et al., 2015) in R version 3.6.3 (R Core Team, 2020). Model selection was based on Akaike's Information Criterion (AIC) and residual standard error. Regression model performance metrics are available in Table S2.

Finally, to describe the distribution of LAI, we measured the percent contribution between measurement heights within the canopy height. This provided a profile describing where most of the leaf area is positioned within canopies.

### 2.4. Emergent leaf area (ELAI) spatial predictions

Our objective was to model ELAI across the marsh using LAI vertical profiles (Section 2.3) and maps of marsh vegetation, elevation, and measured water height. These spatial predictions would then be used to correlate estimated ELAI with measured NEE from the flux tower (Section 2.6) and satellite reflectance data (Section 2.7). This mapping exercise needed to account for changes in elevation and associated water levels relative to the soil surface and the marsh zone canopy type at each point. Therefore, we first mapped our profiles to the marsh landscape by assigning each canopy profile (Eq. 1; Table S3) to its respective marsh zone using an existing habitat map with a spatial resolution of 1 m<sup>2</sup> (Fig. 1c) (Hladik et al., 2013). Areas of the marsh covered by exposed mud or permanent water were not assigned a profile and were given an ELAI value of 0. Classes used were mud, permanent water, marsh interior, mid-marsh, and marsh edges (Fig. 1c).

We measured water level using two pressure transducers (CS456, Campbell Scientific Inc., Logan, UT, USA) located near the flux tower. One pressure transducer was located on the marsh platform at an elevation of 0.88 m NAVD88 approximately 48 m northeast of the tower, and a second in a tidal creek at an elevation of -0.20 m NAVD88 50 m southwest of the tower. Water level elevations were referenced to the vertical datum NAVD88 in units of meters. The pressure transducer on the marsh platform did not capture the full tidal range on the marsh due to its shallow installation within the well. However, the marsh platform did provide a more accurate measurement of marsh surface tidal flooding compared to the sensor in the creek (O'Connell et al., 2017). Therefore, we combined the two measurements to capture the full tidal range and provide a better estimation of marsh flooding (Fig. S1). When the marsh pressure transducer measurement was <0.84 m, we replaced the values with those from the creek pressure transducer.

The next step was to estimate tidal flooding across the marsh surface at any given time for any location within our study area. To do so, we used surface elevations from a digital elevation model (DEM) derived from light detection and ranging (LIDAR) with a 1-m2 horizontal resolution and a vertical accuracy of 0.1 m NAVD88 (Hladik and Alber, 2012) and water level from the pressure transducers. We used a bathtubtype modeling approach to estimate the water level relative to the soil surface based on the DEM and the measured timeseries of water level. For example, a DEM elevation of 0.75 m NAVD88 and a water level elevation of 1 m NAVD88 would give a relative water depth of 0.25 m above the soil surface. This provided a continuous estimate of surface flooding across the marsh. Finally, we used the estimated water level above the soil surface as  $h_x$  in Eq. 1 and used the profile model parameters (Table S3) matching the 1-m<sup>2</sup> area marsh zone (Fig. 1c) to predict ELAI for each location. The results were spatial maps of ELAI for each 30-min measure of water level.

#### 2.5. Flux and environmental measurements

To analyze the correlation between carbon fluxes and estimations of emergent leaf area, we measured atmospheric CO<sub>2</sub> fluxes from an Eddy Covariance (EC) flux tower (31.444, 81.283) at a height of 5 m above the soil surface located 250 m east of the Duplin River (Fig. 1c) using an enclosed-path CO2/H2O gas analyzer (LI-7200, LI-COR Biosciences, Lincoln, NE, USA) and a 3D sonic anemometer (CSAT3, Campbell Scientific Inc., Logan, UT, USA). EC 10 Hz data were processed in EddyPro 7 (LI-COR Biosciences, Lincoln, NE, USA) to 30-min CO2 fluxes representing net ecosystem exchange (NEE). During processing, we conducted double rotation and linear detrending (Wilczak et al., 2001), Webb-Pearman-Leuning correction (Webb et al., 1980), quality control checks (Mauder and Foken, 2006), spectral analysis (Vickers and Mahrt, 1997), high and low frequency spectral corrections (Moncrieff et al., 1997, 2005), and friction velocity filtering and spike removal (Papale et al., 2006). We used data from June October 2020. We conducted our analyses on data that were not gap-filled to reduce any uncertainty related to gap-filling model predictions. Finally, we divided NEE into daytime and nighttime measurements by filtering data according to the modeled solar elevation angle (nighttime 20; daytime 30) using the R package maptools (Bivand and Lewin-Koh, 2022). Further, for daytime measurements, we filtered data to include those with photosynthetically active radiation (PAR) 500 mol CO<sub>2</sub> m <sup>2</sup> s <sup>1</sup> using a quantum sensor (LI-190R, LI-COR Biosciences, Lincoln, NE, USA). We did this to reduce NEE variability caused by shoulder periods around morning and evening times and large changes in radiation intensity from cloud cover. Additional environmental variables were collected at the tower including air temperature and relative humidity (HMP45C, Campbell Scientific Inc., Logan, UT, USA) and soil temperature (TCAV-L, Campbell Scientific Inc., Logan, UT, USA). We used air temperature and relative humidity to calculate vapor pressure deficit (VPD) following Bolton (1980).

### 2.6. Footprint analysis

We used EC based footprint analysis to generate spatial predictions of flux source areas every 30 min to match the NEE measurements (Kljun et al., 2015). We used these spatial predictions to link measured NEE from the flux tower with marsh surface characteristics including emergent leaf area during tidal flooding. Flux footprint predictions (FFP), the spatial predictions of flux source areas, were generated in *R* version 3.6.3 (R Core Team, 2020) (Kljun et al., 2015). For FFP generation, input variables needed were sensor height, wind speed, wind direction, friction velocity (u\*), Obukhov length, and the standard deviation of the lateral velocity fluctuations. These were obtained from EddyPro 7 processed fluxes all at the timescale of 30 min. An additional variable, boundary layer height (BLH), was retrieved from the Modern-Era Retrospective analysis for Research and Applications version 2

(MERRA-2) hourly time-averaged 2-dimensional data single-level dataset (MERRA-2 tavg1\_2d\_slv\_Nx) (Global Modeling and Assimilation Office (GMAO), 2015). A single pixel covering our study site, with a spatial resolution of  $0.5 \times 0.625$ , was chosen. The hourly data from this pixel, spanning our study period, was extracted, and an hourly time series of BLH was produced. We linearly interpolated the hourly time series into 30-min intervals to match our flux data resulting in each FFP having a corresponding BLH measurement. We generated FFPs (n 2559; day 1823; night 736) with 90% source areas and their footprint function values (FFV), the estimated contribution of each 1 m<sup>2</sup> area within the FFP to the NEE measurement (Fig. S2). FFPs were filtered to those with lengths between 75 and 600 m and a circularity 0.3. Lastly, we excluded any measurements where FFPs intersected with the nearby Duplin River. These filtering criteria were used to remove generated FFPs with implausible shapes and to restrict the analysis to a defined area. We also generated a yearly climatology (Fig. S3) to select satellite pixels for comparing LAI to satellite reflectance.

To explore the relationship between spatial estimations of ELAI (Section 2.4) and NEE, we overlayed the FFP corresponding to each 30-min NEE measurement on to our spatially explicit ELAI maps that represent flooding conditions during the same 30-min period. However, within each FFP, areas closer to the flux tower had higher influence on measured NEE and this proportion of influence was represented by the FFV (Kljun et al., 2015). The sum of the FFVs within an FFP equals the source area contribution (90%). An example of an FFP with its FFVs is provided in Fig. S2. We therefore summarized the ELAI within each FFP by calculating the weighted sum of ELAI using the FFVs as weights, which was then normalized by the area of the FFP to derive emergent leaf area index per unit FFP (ELAI<sub>FFP</sub>). The ELAI<sub>FFP</sub> can be summarized as follows, for each j FFP with an area of  $A_j$ :

where i is each unit area within the FFP with an ELAI value  $x_i$  and a corresponding FFV weight  $w_i$ .

We estimated the amount of tidal flooding within each FFP by measuring the weighted mean of water level relative to the soil surface using the FFV as weights. This allowed us to determine when the marsh was flooded within each FFP. In summary, for each FFP which represented the source area for each 30-min NEE measurement, we modeled the amount of ELAI within the FFP area (ELAI<sub>FFP</sub>) using our marsh zone specific profiles, DEM, and pressure transducer water level.

### 2.7. Satellite remote sensing reflectance

Our last objective was to relate satellite surface reflectance with our modeled ELAI. We acquired Sentinel-2 Level-2A surface reflectance from Google Earth Engine (Gorelick et al., 2017) for the study period (June October 2020). We retained ten scenes for use (Table S4) after filtering for clouds via the Copernicus Cloud Probability band. We selected pixels from within the yearly climatology (Fig. S3) (*n* 2097). For each pixel and scene, we calculated vegetation indices listed in Table S5.

To compare Sentinel-2 vegetation indices with our modeled ELAI, we scaled ELAI estimations from the original 1-m to the 10-m resolution to match Sentinel pixels. To do this, we overlayed the Sentinel pixel grid (Fig. S2) on the habitat map and used the number of pixels per habitat class that fell in each Sentinel pixel as weights. We then calculated the weighted mean of ELAI within each pixel based on our modeling approach found in Section 2.6 but substituting the proportion of habitat class and its calculated ELAI within each Sentinel pixel in place of the FFV. We measured the mean elevation within each pixel to derive perpixel elevation values. We then classified each Sentinel-2 pixel based on its LAI<sub>max</sub> (3 classes) and the water level height as predicted by our

bathtub model (5 classes in 0.1-m intervals). We then grouped similarly classified pixels and measured their mean  $\rm LAI_{max}$ ,  $\rm ELAI$ , and vegetation index values.

We used linear regression to estimate both ELAI and  $LAI_{max}$  for each vegetation index listed in Table S5. This allowed us to compare whether vegetation indices could predict reduced leaf area due to tidal flooding. To select the best linear models, we split the data into training (75%) and testing (25%) datasets, where we relied on a stratified sampling of Sentinel-2 scene dates to derive the split. Within the training data, for each index, we performed 3-fold cross-validation and selected the best performing model based on root mean square error (RMSE) from the three folds. We then tested each of the selected vegetation index models on the testing data to determine which index was the best predictor of ELAI and LAI $_{max}$ . We measured model performance by regressing predicted values on observed values and using the coefficient of determination ( $R^2$ ), normalized RMSE (NRMSE) (Eq. 2), and the slope and intercept coefficients as goodness-of-fit metrics. NRMSE was calculated as follows:

where  $x_{max}$  and  $x_{min}$  are the maximum and minimum of the observed values, representing the range. For training linear models, we used the Tidymodels suite of packages (Kuhn and Wickham, 2020) in R version 3.6.3 (R Core Team, 2020).

Finally, we compared our spatial ELAI estimations to MODIS 8-day LAI products (MYD15A2H). We retrieved MYD15A2H and the 8-day reflectance product (MYD09A1) from Google Earth Engine (Gorelick et al., 2017). We used MYD90A1 to determine the overpass date window of the 8-day products as this information is not available in the MYD15A2H product (Myneni et al., 2015). We did so to match our ELAI estimations with MODIS 8-day overpass times. To scale our ELAI to MODIS pixels, we followed the same procedure as with Sentinel-2. Details of MODIS pixel spatial and temporal coverage over our study site and pixels used in analysis can be found in Fig. S9 and Table S6.

Throughout, we report means and standard errors (SE) except where otherwise indicated, and tested differences between groups using Kruskal-Wallis tests and pairwise comparisons using Wilcoxon rank sum tests in *R* version 3.6.3 (R Core Team, 2020).

### 3. Results & discussion

### 3.1. Leaf area index and vertical profiles

Our in situ LAI measurements at permanent vegetation plots varied significantly at fine spatial scales. Maximum canopy LAI (LAI $_{max}$ ), the total LAI of the canopy under non-flooded conditions, varied across an elevation gradient from tall and sparse canopies with high LAI (height: 1.23 0.16 m; density: 77 22 stems m  $^2$ ; LAI $_{max}$ : 3.19 1.01) found at low elevation marsh edges, to shorter and denser canopies with lower LAI (height: 0.47 0.10 m; density: 316 108 stems m  $^2$ ; LAI $_{max}$ : 1.28

0.04) in the higher elevation marsh interior (Table 1). Mid-marsh canopies had the lowest LAI but intermediate canopy heights and densities (height: 0.68 0.12 m; density: 174 60 stems m<sup>2</sup>; LAI<sub>max</sub>: 1.03

 $\label{thm:continuous} \textbf{Table 1} \\ \textbf{Means and standard deviations for maximum Leaf area index (LAI_{max}), stem density, and canopy height \textit{S. alterniflora} zones from vegetation plots for data collected from June through October 2020. \\ \end{aligned}$ 

Canopy	Leaf Area Index (m <sup>2</sup> m <sup>2</sup> )		Stem Density (# stems m <sup>2</sup> )		Canopy Height (m)	
edge mid-	3.19	1.01	77	22	1.23	0.16
marsh	1.03	0.39	174	60	0.68	0.12
interior	1.28	0.40	316	108	0.47	0.10

0.39

Our field measurements of canopy characteristics across the marsh elevation gradient demonstrated large differences across short distances (Fig. 3a). For areas of the marsh just meters apart, canopy height, stem density, and LAI varied up to 89%, 102%, and 122%, respectively (Table 1). Our results mimic the negative relationship between canopy height and stem density in tidal marshes that follows the self-thinning law related to resource competition (Chaisson et al., 2022; Gorham, 1979; Liu and Pennings, 2019). We also found LAI is not linearly related to canopy height, and structural changes in canopies are associated with both stem height and density (Fig. S5). The canopy architecture of marsh grass species, such as S. alterniflora, tends to have erectophile stems (Kearney et al., 2009). This is evident in the marsh interior, where stems are short and vertical with high density. However, in lower elevation marsh edges, plant canopy architecture becomes more planophile, increasing LAI. Our findings suggest significant canopy heterogeneity across elevation gradients that will impact LAI estimations, particularly when scaling through remote sensing methods. This will further be impacted by tidal flooding, where emergent leaf area will be dependent on elevation and canopy architecture.

We also found variability in the vertical profiles of LAI (Fig. 2), which influence emergent LAI during tidal flooding. We measured LAI at intervals from the soil surface to the canopy top in tall marsh edge canopies (0.2 m intervals) and short mid-marsh and interior marsh canopies (0.1 m intervals). For mid-marsh and interior canopies, a larger proportion of the total LAI was positioned lower in the canopy ( 30% of the total canopy height). Taller marsh-edge canopies had the majority of total LAI distributed mid-height within the canopy profile (30 60% of total canopy height) (Fig. 2a).

We modeled these LAI measurements as a function of canopy height to determine the vertical cumulative distribution of LAI. This allowed us to predict ELAI during flooding events (Figs. 2b &2c). We found that the Weibull Type-1 3-parameter cumulative distribution function, widely used in forest canopy modeling (Teske and Thistle, 2004; Yang et al., 1993), was the best fit for marsh canopy LAI (Tables S2 and S3). Again, for plants just meters apart (marsh edge vs. interior), LAI profiles showed differences in the overall shape (Fig. 2a) and cumulative distribution of LAI (Fig. 2b) within the canopies (Fig. 3a). Shorter canopies in the marsh interior had the majority of LAI positioned lower in the canopy compared to the taller plants in the mid-marsh and marsh edge, which had a more spread-out distribution (Fig. 2a).

The normalized profiles provided a direct comparison of leaf area cumulative distribution relative to canopy height and LAI<sub>max</sub> (Fig. 2c). For example, at water level height of 50% of the canopy height, taller marsh edge plants ( 1 m) had 27% of the canopy LAI emergent, while shorter plants in the interior marsh areas had from 13% (mid-marsh) to 7% (interior) emergent. These data show that leaf area profile shapes are dependent on canopy height, and the relative water height will impact emergent leaf area differently across the marsh gradient. In other studies, differences in light attenuation through canopies and canopy LAI profiles have shown differences across marsh grass species (Kearney et al., 2009; Ramsey et al., 2004). Our findings suggest there is withinspecies variation in vertical LAI distributions that are dependent on canopy height, which varies across environmental gradients. This is important to consider since tidal salt and brackish marshes tend to be monocultures and illustrates the heterogeneity of canopy leaf area across a single species, as we show here, as well as across different marsh grass species.

### 3.2. Net ecosystem exchange (NEE) and emergent leaf area

The spatial extent of *S. alterniflora* LAI<sub>max</sub> across the marsh and within our flux tower footprint was highly variable (Fig. 3b) and demonstrates the heterogeneity within these monoculture ecosystems. The majority of marsh canopy sampled by the flux tower consisted of mid-

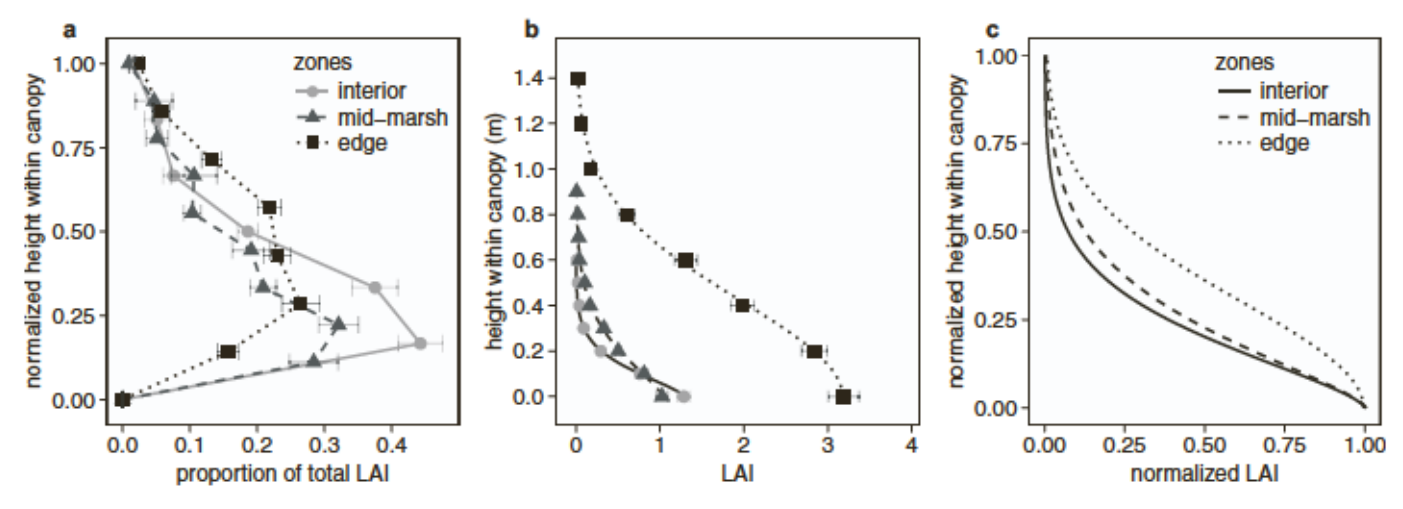


Fig. 2. a) Canopy profiles of leaf area index (LAI) showing the proportion of LAI through the canopies of marsh interiors (solid), mid-marshes (dashed), and edges (dotted). b) Cumulative distributions of LAI and c) normalized by canopy height and total LAI. Lines in plots b and c are Weibull Type-1 model fits. Points for all plots are means with standard error bars. Note, axes for b and c are flipped for clearer interpretation.

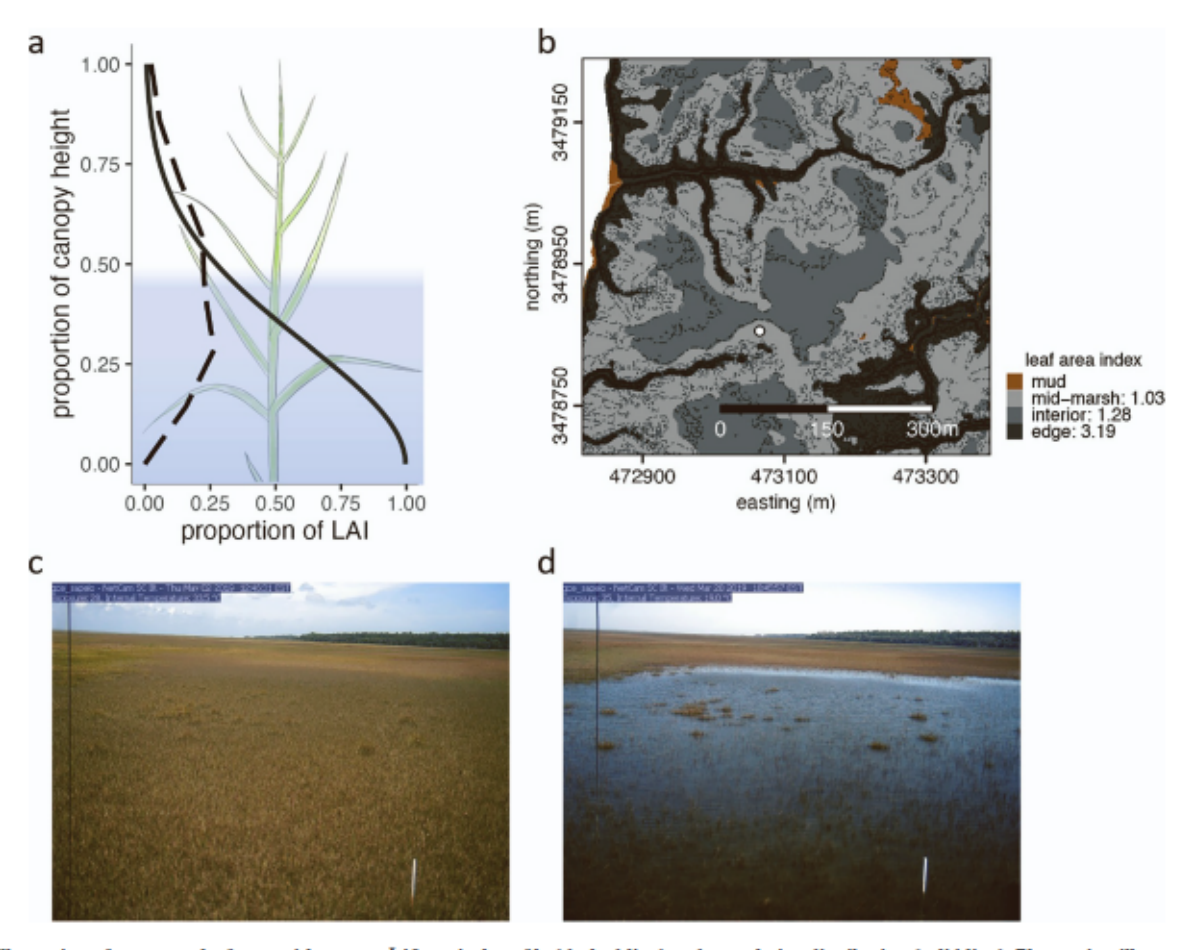


Fig. 3. a) Illustration of emergent leaf area with canopy LAI vertical profile (dashed line) and cumulative distribution (solid line). Blue region illustrates portion of canopy flooded by tidal waters. b) Map of the leaf area index (LAI) for S. alterniflora around the flux tower. White point is the location of the GCE LTER flux tower. Photographs from a PhenoCam installed on the GCE LTER flux tower capturing c) non-flooded and d) flooded periods in the S. alterniflora marsh. (For interpretation of the references to colour in this figure legend, the reader is referred to the web version of this article.)

marsh and interior plants which have lower LAI (range: 0.93 to 1.16). During tidal flooding, ELAI was variable and dependent on elevation and canopy architecture (Fig. 3b) and was unevenly reduced across the marsh (Figs. 4a-4e). For example, for a tide elevation measurement of 1.3 m NAVD88, the amount of ELAI could range from <0.3 in the

interior to >1 along the marsh edges (Fig. 4b) and the proportion of submerged LAI was dependent on canopy type and elevation (Fig. 2a). This observed heterogeneity in canopy flooding, therefore, will impact eddy covariance flux tower source areas, FFPs, and their measured atmospheric carbon fluxes, NEE.

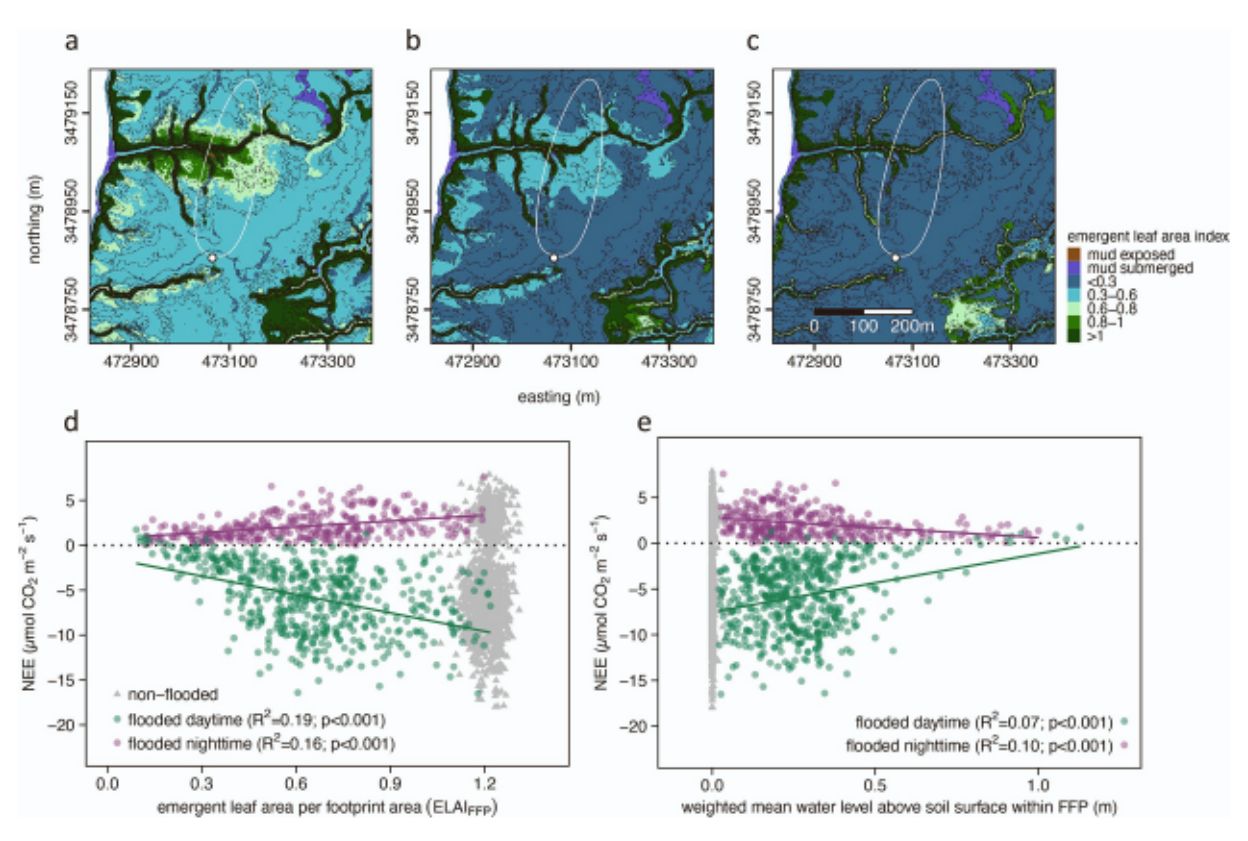


Fig. 4. a-c) Maps of the flux tower area illustrating the emergent leaf area under three tide heights: a) 0.25 m relative to soil surface at the tower (1.25 m NAVD88), b) 0.50 m (1.3 m NAVD88), and c) 0.75 m (1.55 m NAVD88). Mudflats are represented as exposed or submerged. White oval is an example 30 min flux footprint prediction (2020-06-15 19:30 UTC + 0), white point is the flux tower location, and dashed lines are 0.1 m elevation contours. d) Net ecosystem exchange (NEE) as a function emergent leaf area index per footprint area (ELAI<sub>FFP</sub>) and e) NEE as a function of the weighted mean of water level relative to the soil surface within each FFP. Green points are for daytime measurements with tidal flooding, purple points are nighttime measurements during tidal flooding, and gray triangles are measurements during non-flooded periods. Lines are linear regression fits to the tidal flooding data only separated by daytime and nighttime.

Flux tower-measured 30-min NEE, where negative values indicate C uptake by the marsh, showed a significant relationship (daytime: R<sup>2</sup> = 0.19, p < 0.001; nighttime:  $R^2 = 0.16$ , p < 0.001) with ELAI<sub>FFP</sub> only during tidal flooding periods (Fig. 4d). The correlation between NEE and ELAIFFP was higher than that between NEE and a spatial estimation of marsh surface flooding using the weighted mean water level within each FFP (daytime:  $R^2 = 0.07$ , p < 0.001; nighttime:  $R^2 = 0.10$ , p < 0.001) (Fig. 4e) and to the measured water level at the flux tower as a point measurement (daytime:  $R^2 = 0.15$ , p < 0.001; nighttime:  $R^2 = 0.11$ , p < 0.001). From dry conditions (ELAI<sub>FFP</sub> > 1) through a reduction of ELAI<sub>FFP</sub> to 0.6 (a 40% reduction in ELAI), daytime mean NEE remained nearly constant, ranging from -6.53 to -7.64 µmol CO<sub>2</sub> m<sup>-2</sup> s<sup>-1</sup> (Fig. 4d; Table 2). However, once canopy ELAIFFP reached below 0.6, mean daytime NEE dropped by 25% (-4.91  $\pm$  0.25  $\mu$ mol CO<sub>2</sub> m<sup>-2</sup> s<sup>-1</sup>). Further, when ELAI<sub>FFP</sub> decreased to <0.3, mean NEE was  $-0.93\pm0.25$ µmol CO2 m<sup>-2</sup> s<sup>-1</sup>, a decrease of 87% compared to non-flooded conditions (Table 2). Nighttime NEB, representing ecosystem respiration (Re), had a lower correlation with ELAIFFP compared to daytime measurements (Fig. 4d). However, Re in most ecosystems is predominately controlled by temperature (Lloyd and Taylor, 1994). During our study period and after rigorous filtering (see Sections 2.5 & 2.6), tidal flooding conditions where canopy ELAIFFP was below 0.6 (where significant declines in NEE were measured) occurred 16% of the time. However, marsh flooding frequency and magnitude change seasonally with more frequent marsh flooding occurring from August through November (Narron et al., 2022).

Our comparison of NEE correlations to ELAIFFP and water level suggest that spatially modeling marsh flooding and the associated reduction in emergent leaf area is an improvement over water level measurements at a single point (Fig. 4d & 4c). That is because tidal

Table 2 Descriptive statistics for daytime and nighttime EC flux tower net ecosystem exchange (NEE;  $\mu$ mol CO $_2$  m $^{-2}$  s $^{-1}$ ) grouped by classes of emergent leaf area index per flux footprint prediction (ELAI<sub>FFP</sub>). The column titled Significance from > 1 (no flooding) are p-values from pairwise Wilcoxon rank sum tests indicating each flooded group's difference from conditions with no flooding.

Period	ELAI <sub>PP</sub>	NEE mean ± standard error	Minimum	Maximum	Significance from >1 (no flooding)
		$-0.93 \pm$			
daytime	<0.3	0.25 -4.91 ±	-6.28	1.74	<0.001
	0.3-0.6	0.25 -6.53 ±	-14.29	0.68	< 0.001
	0.6-0.8	0.25 -7.64 ±	-16.40	0.33	0.09
	>0.8	0.33	-16.51	1.25	0.04
	>1 (no	$-6.97 \pm$			
	flooding)	0.11 1.24 ±	-17.99	1.58	-
nighttime	<0.3	0.12 1.74 ±	0.08	3.2	<0.001
	0.3-0.6	0.1 2.25 ±	0.22	6.57	< 0.001
	0.6-0.8	0.15 2.89 ±	0.01	6.14	< 0.001
	>0.8 >1 (no	0.16 3.12 ±	0.36	7.59	0.17
	flooding)	0.07	0.06	7.89	_

flooding in marshes is spatially variable and often regulated by local elevation, wind speed, and wind directions. Similarly, tidal marsh NEE is often controlled by several environmental drivers including incident PAR, air and soil temperature, vapor pressure deficit (VPD), and tidal water level (Hawman et al., 2021; Knox et al., 2018). Therefore, a single parameter cannot accurately predict tidal marsh NEE and the compounding effects of frequent and variable tidal flooding can have varying impacts on NEE and associated drivers (Forbrich and Giblin, 2015; Kathilankal et al., 2008; Knox et al., 2018; Moffett et al., 2010) which makes modeling challenging (Wood, 2022). At our site, ELAIFFP estimations showed comparable relationships to NEE as other drivers such as PAR under tidal flooding conditions (Fig. S6) and a better correlation than water level measured at single point at the flux tower or a spatial prediction of water level over the marsh surface within FFPs (Figs. 4d & 4e). This suggests improvements in modeling NEE could be made for salt marshes by focusing on canopy dynamics related to changes in flux footprints and changes in leaf area from tidal flooding within those footprints. Although our results indicate some improvements at the flux tower scale (Figs. 4d & 4e), sources of uncertainty include linking spatially heterogeneous canopying flooding within footprints to single

NEE reductions under tidal inundation are often attributed to combinations of plant metabolism inhibition and temperature changes (Moffett et al., 2010); reduced light interception in flood waters (Kathilankal et al., 2008; Nahrawi et al., 2020); physical submergence (Kathilankal et al., 2008; Moffett et al., 2010; Nahrawi et al., 2020); and soil flooding (Pezeshki, 1997). We expected NEE reductions to be more sensitive to canopy submergence than was observed. A possible explanation could be within canopy vertical gradients of stomatal conductance driven by temperature, vapor pressure, and saturation deficit (Jarvis and McNaughton, 1986). Higher rates of stomatal conductance at the tops of canopies could explain the insensitivity of NEE. To test this hypothesis, we need leaf level measurements of stomatal conductance at varying heights within marsh canopies.

Our findings on tidal marsh NEE sensitivity to tidal flooding were similar to previous studies (Forbrich and Giblin, 2015; Kathilankal et al., 2008; Moffett et al., 2010; Nahrawi et al., 2020). However, these studies only looked at water level height relative to canopy height and did not account for emergent leaf area changes. Forbrich and Giblin (2015) and Kathilankal et al. (2008) measured decreases in NEE when water level heights reached 0.05 m and 0.25 m, respectively. The higher sensitivity to flooding observed by Forbrich and Giblin (2015) was attributed to the low canopy height of *S. patens* and its prostrate habit. Nahrawi et al. (2020) reported that NEE sensitivity to flooding varied through time at our site based on ratios of water height to canopy height. Additionally, Kathilankal et al. (2008) and Moffett et al. (2010) reported abrupt changes in NEE when water heights reached ~40% of the plant stem heights for *S. alterniflora* and *S. foliosa*, respectively.

Varying LAI profiles and cumulative distributions across canopy height (this study) and across species (Kearney et al., 2009; Ramsey et al., 2004) could explain the range of sensitivities to flooding seen in the literature. Our normalized LAI profiles illustrated the dependence of ELAI on flooding height and position within the marsh elevation gradient (Figs. 2c & 3b). Thus, with canopies flooded to 50% of their total height, short dense stems in the marsh interior had only 7% of their total LAI emergent, while tall plants at the creek edge had 27%. Further, we would expect this variability to increase as canopy phenology and species differences are considered, which should increase the need to account for LAI variation in downstream modeling. For example, NEE models will need to account for the significant change in marsh surface characteristics that cause spatial variation in flooding heights (Fig. 4a-3c) and concomitant variation in emergent LAI in flux tower FFPs, as these flooding patterns within a particular flux source area impact measured fluxes (Fig. 4d). Linking more precise estimations of canopy flooding in salt marshes may improve our understanding of the carbon assimilation responses to long and short-term disturbances. Salt marsh

surface characteristics are subject to rapid changes from vertical marsh accretion or subsidence (Schuerch et al., 2018), wrack and debris deposition (Reidenbaugh and Banta, 1980), erosion on the marsh surface by tides, lateral marsh erosion from wave action (Kirwan et al., 2016), as well as creek migration (Crotty et al., 2020; Hughes et al., 2009). These surface changes occur at a variety of time scales, ranging from daily tidal flooding to annual cycles, and they all may alter the flooding and drainage patterns. Further spatiotemporal differences in emergent vegetation should be more directly related to NEE than flooding per se. We, therefore, conclude that estimations of emergent LAI would improve predictions of NEE when implemented in production models and would be sensitive to flux source areas.

#### 3.3. Satellite products and emergent leaf area

Our last objective was to determine the feasibility of estimating ELAI using satellite reflectance only. Doing so would improve the scalability of emergent leaf area outside a flux tower footprint with known vegetation distribution, water level, and elevation. This would allow ELAI to be applied to new locations and be based on current conditions without relying on existing vegetation maps and DEMs (i.e., canopy density distribution).

LAI is often predicted from satellite data (Boresjoe Bronge, 2004) and we show here that we can further predict the more dynamic ELAI in tidal marshes. Based on Sentinel-2 10-m resolution data with a 5-day revisit period, we captured a range of tidal flooding events around our flux tower (Table S4), allowing us to model ELAI from surface reflectance. We regressed vegetation indices (Table S5 and Fig. S7) on our spatial predictions of ELAI around the flux tower (Fig. S2) and found the nearinfrared reflectance of vegetation (NIR<sub>V</sub>) index (Badgley et al., 2017) was the best predictor of ELAI ( $R^2$  0.89; NRMSE 9.9%; slope 0.87; intercept 0.21) (Fig. 5a and Table S5). In general, vegetation indices that use near-infrared (NIR) bands were better predictors than those based only on visible bands (Table S5). This is in part because tidal flooding changes the observed canopy architecture and density, which NIR is sensitive to (Kearney et al., 2009). Previous studies have indicated this as a challenge to mapping tidal marsh biomass (Ghosh et al., 2016; Kearney et al., 2009). However, we show here that this sensitivity to canopy submergence can be successfully used to predict ELAI. As a comparison, we tested predicting  $LAI_{max}$ , without accounting for flooding, using vegetation indices and found poor results (Fig. S8 and Table S5).

The ability to predict ELAI from satellite data has strong implications for research related to regional productivity modeling and carbon assimilation. Often, moderate resolution productivity estimates measure 8-day summations of assimilated carbon (Ge et al., 2016; Kang et al., 2018; Tao et al., 2018; Wu et al., 2015). However, because the timing and amplitude of tides varies through time, their impact on total assimilated carbon for an 8-day period will also vary. Our EC measures of NEE show a dependence on tidal submergence (Fig. 4d). When considering the two-hour window centered on Sentinel-2 overpasses (16:00 UTC 0) for a dry (August 26, 2020) and flooded day (September 5, 2020), the dry mean NEE was significantly higher in magnitude ( 9.63 1.24 mol  $CO_2$  m  $^2$  s  $^1$ ) than the flooded ( 4.320.16 mol  $CO_2$  m  $^2$  s  $^1$ ) (Fig. 5c & 4d). Therefore, linking ELAI with carbon assimilation rates may improve our ability to model tidal marsh productivity at larger spatial scales and account for variation due to tidal activity.

ESMs and productivity models frequently rely on coarser resolution satellite data such as MODIS (Hu et al., 2022). To determine whether the standard MODIS LAI product MYD15A2H (an 8-day composite at the 500-m pixel scale) was a good measure of ELAI, we scaled ELAI spatial estimations to MODIS pixel areas and compared them to MYD15A2H. We found that MYD15A2H overestimated LAI (7 93%) when median water levels above the soil surface were 0.15cm within pixel areas (Fig. 5b). During drier conditions (0.15 m), MYD15A2H

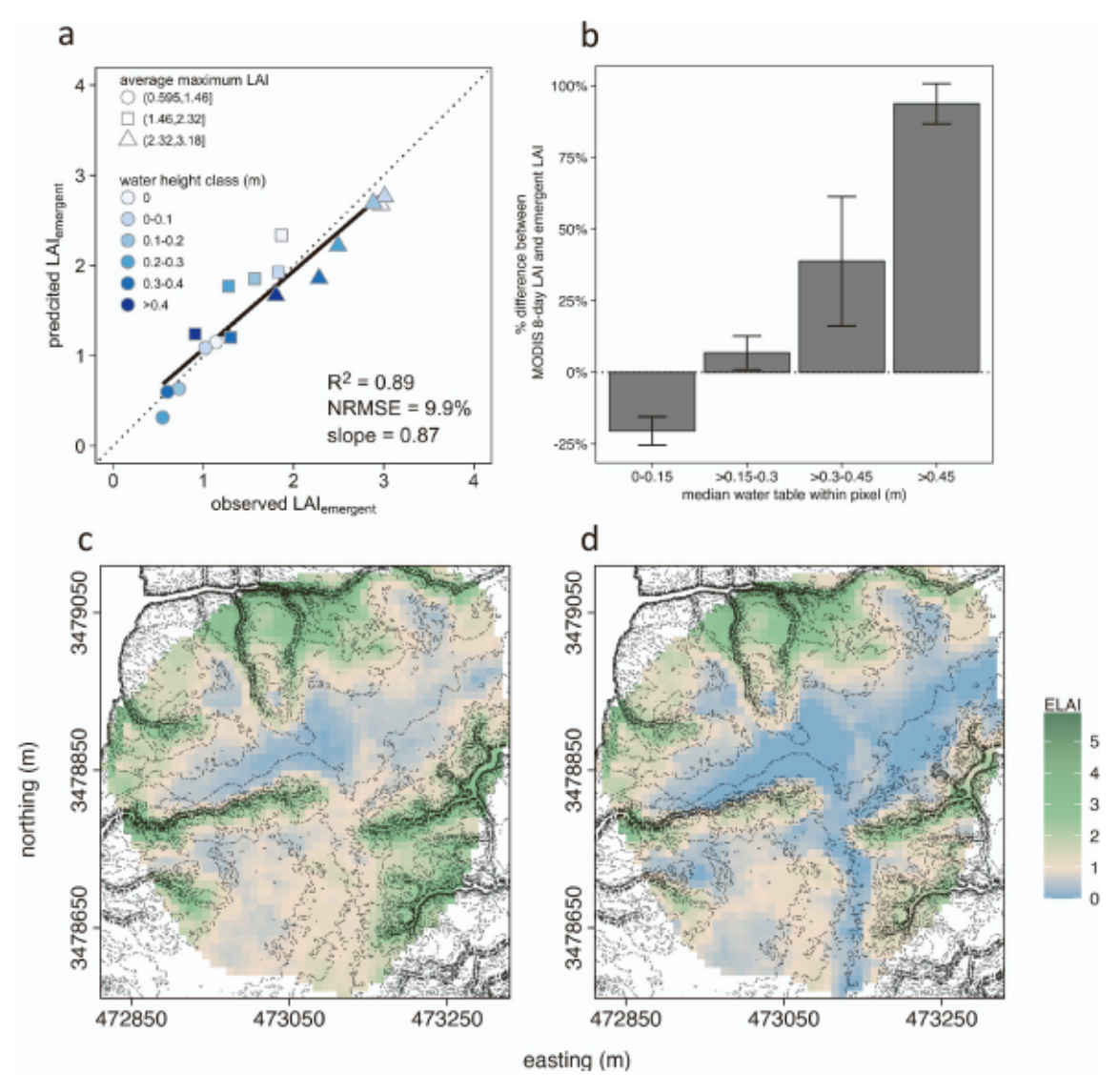


Fig. 5. a) Performance plot and metrics using Sentinel-2 derived near-infrared reflectance of vegetation (NIR<sub>W</sub>) to predict emergent LAI (ELAI). Data presented are the hold-out testing dataset not seen during the linear regression model training. Points are colored by the assigned water level classes representing the average water height relative to the soil surface within pixels. Point shapes represent mean LAI<sub>max</sub> ranges within pixels. Metrics reported are the coefficient of determination (R<sup>2</sup>), normalized root mean square error (NRMSE), and the slope of regression between predicted and observed. b) The percent differences between MODIS 8-day LAI estimates (MYD15A2H) and pixel averaged ELAI across water level heights relative to the soil surface for five MODIS pixels around the study location. Error bars represent standard errors. c-d) Sentinel-2 predicted emergent leaf area index (LAI) using the near-infrared reflectance of vegetation (NIR<sub>W</sub>) index for two example overpass days: c) August 26, 2020, with a mean water level height of 0 m (range: 0–0.174 m) and d) September 5, 2020, with a mean water level height of 0.16 m (range: 0–1.19 m) above soil surface. White point indicates flux tower location, the area of Sentinel-2 predicted ELAI are the flux yearly climatology, and dashed lines are 0.1 m elevation contours.

underestimated LAI by ~20%. We found that NIR<sub>V</sub> calculated from MODIS reflectance data had a better relationship ( $R^2 = 0.25; p < 0.001$ ) with ELAI compared to MYD15A2H ( $R^2 = 0.07; p < 0.03$ ) (Fig. S10). The poorer correlation with the MYD15A2H product could be attributed to the radiative transfer models used (Knyazikhin et al., 1998), which lack wetland specific look-up-table parameters (Myneni et al., 2015), and do not consider tidal flooding. These results present uncertainty in moderate resolution studies that rely on LAI estimations for productivity modeling for tidal marshes. Our ELAI spatial estimations showed improvements at these moderate scales, but future work should focus on determining the impacts heterogeneous canopy flooding has on scaling leaf area estimations to coarser resolutions.

Our results show that surface reflectance from satellite data can be used to quantify emergent leaf area during tidal flooding. At our study site, the vegetation index NIR<sub>V</sub> correlated well with our marsh canopy type (species and density). However, we expect the relationship between ELAI and vegetation indices to vary across sites and canopy composition (e.g., species). Future research should include the feasibility of estimating emergent leaf area in other tidal wetland types. Additionally, assessing the impact of incorporating ELAI in production models is needed.

### 4. Conclusion

Tidal marshes are ecosystems where canopy leaf area varies over 3-fold for areas just meters apart. In addition to this high spatial variability, frequent tidal flooding introduces a temporal component that alters emergent leaves at short timescales, e.g., hourly. We show that by modeling the vertical distribution of LAI within tidal salt marsh canopies, we can predict emergent leaf area across landscapes and tidal cycles. We found an improved relationship between NEE and ELAI ( $R^2 = 0.19$ ) compared to NEE and surface flooding estimations alone. This

improvement indicated that NEE under tidal flooding was driven more by emergent leaf area and not the magnitude or presence of tidal flooding, per se. Rather, NEE responded to flooding only if changes in ELAI occurred. This would be dependent on the canopy height and density and location within the tidal frame. Further, we showed that ELAI could be estimated through remote sensing data. This will create a better understanding of functions that depend on leaf area, such as carbon exchange. Our estimates are an improvement over the existing moderate resolution LAI product (MYD15A2H), which showed significant uncertainty in LAI estimations that could be negatively impacting productivity modeling for assessing blue carbon stocks and ESMs for modeling the movement of carbon.

Long-term and broad-scale monitoring of blue carbon within coastal salt and brackish marshes require precise information regarding biophysical characteristics such as LAI and productivity metrics such as NEE and GPP. The MODIS GPP product (MOD17) is a powerful tool for estimating broad-scale blue carbon budgets but does not apply to wetland vegetation because of the lack of wetland-specific look-up-table (LUT) values (Myneni et al., 2015; Running et al., 2004; Running and Zhao, 2015). Therefore, there is a need to utilize lessons learned from existing flux tower-based marsh NEE and GPP models and use them to develop satellite-based methods to study the broad-scale, long-term trajectories of coastal marsh plant GPP or carbon storage capacity. Our proposed method will help to accurately estimate one of the biophysical parameters, LAI, which is fundamental for NEE and GPP models. The variable nature of LAI in tidal wetlands needs to be built-in to future satellite-based modeling efforts to address one significant source of uncertainty, which is the variability induced in the datasets due to the fluctuation in tidal flooding during satellite overpasses. We encourage researchers in other tidal wetland ecosystems to consider the impact ELAI has on their ecosystem models.

This study has several broader implications, including increasing our predictive capacity to model CO2 exchange after natural and anthropogenic disasters, understanding carbon sources and sinks within coastal marshes, and use by coastal managers to assess restoration success and trajectories for critical coastal ecosystems. The ability to estimate emergent leaf area may have applications outside of productivity modeling. As rates of sea-level rise increase along with coastal flooding (Vitousek et al., 2017), tidal marshes must keep pace through vertical accretion and landward migration (Kirwan et al., 2016; Schuerch et al., 2018). Time-series of emergent leaf area and the frequency and intensity of daily tidal inundation could provide insight into tidal marsh responses to sea-level rise, and structural shifts in marsh canopies may provide an early warning of changing environmental gradients. Further, impacts on marsh geomorphology, such as creek migration caused by local disturbances including grazing and burrowing (Crotty et al., 2020; Wu et al., 2021) or anthropogenic eutrophication (Deegan et al., 2012) could be investigated through improved canopy modeling. Future research should focus on relating emergent leaf area with other ecosystem functions and processes across species and environmental gradients to improve our understanding of marsh canopy carbon dynamics, marsh resiliency, and habitat structure for dependent species.

### Credit author statement

**Peter A. Hawman:** Conceptualization, Analysis, Satellite data processing, Modeling, Writing, Editing. **Deepak R. Mishra:** Conceptualization, Editing, Reviewing, Overall supervision. **Jessica L. O'Connell:** Editing, Reviewing, Overall supervision.

### **Declaration of Competing Interest**

The authors declare that they have no known competing financial interests or personal relationships that could have appeared to influence the work reported in this paper.

### Data availability

Data will be made available on request.

### Acknowledgments

This research was supported by NASA (Carbon Cycle Science #NNX17AI76G) and the NSF (Georgia Coastal Ecosystems LTER OCE-1237140 and OCE1832178) projects. The authors would like to thank Merryl Alber, Jacob Shalack, Dontrece Smith, Elise Diehl, John Williams, Adam Sapp, and Wade Sheldon and for field transportation and logistics and for flux tower data collection, sensor maintenance, and data management at the GCE LTER site. We would also like to thank Tyler Lynn, Asa Julien, Jan Veerman, Jessica Turner, and Caroline Narron for their help in collecting field data. This is contribution 1113 of the University of Georgia Marine Institute.

#### Appendix A. Supplementary data

Supplementary data to this article can be found online at https://doi.org/10.1016/j.rse.2023.113553.

### References

- Asner, G.P., Scurlock, J.M.O., Hicke, A., J., 2003. Global synthesis of leaf area index observations: implications for ecological and remote sensing studies. Glob. Ecol. Biogeogr. 12, 191 205. https://doi.org/10.1046/j.1466-822X.2003.00026.x.
- Badgley, G., Field, C.B., Berry, J.A., 2017. Canopy near-infrared reflectance and terrestrial photosynthesis. Sci. Adv. https://doi.org/10.1126/sciadv.1602244.Bivand, R., Lewin-Koh, N., 2022. maptools: Tools for handling spatial objects (manual).
- Bolton, D., 1980. The computation of equivalent potential temperature. Mon. Weather Rev. 108, 1046–1053. https://doi.org/10.1175/1520-0493(1980)108–1046: TCOEPT 2.0.CO;2.
- Boresjoe Bronge, L., 2004. Satellite remote sensing for estimating leaf area index, FPAR and primary production. A literature review.
- Cai, W.-J., Pomeroy, L.R., Moran, M.A., Wang, Y., 1999. Oxygen and carbon dioxide mass balance for the estuarine-intertidal marsh complex of five rivers in the southeastern U.S. Limnol. Oceanogr. 44, 639 649. https://doi.org/10.4319/ lo.1004.44.2.0620
- Chaisson, C., Jones, C.C., Warren, R.S., 2022. Seasonal stem loss and self-thinning in low marsh Spartina alterniflora in a New England tidal marsh. Estuar. Coasts. https://doi.org/10.1007/s12237-022.01054.0
- Chapin, F.S., Woodwell, G.M., Randerson, J.T., Rastetter, E.B., Lovett, G.M., Baldocchi, D.D., Clark, D.A., Harmon, M.E., Schimel, D.S., Valentini, R., Wirth, C., Aber, J.D., Cole, J.J., Goulden, M.L., Harden, J.W., Heimann, M., Howarth, R.W., Matson, P.A., McGuire, A.D., Melillo, J.M., Mooney, H.A., Neff, J.C., Houghton, R.A., Pace, M.L., Ryan, M.G., Running, S.W., Sala, O.E., Schlesinger, W.H., Schulze, E.-D., 2006. Reconciling carbon-cycle concepts, terminology, and methods. Ecosystems 9, 1041 1050. https://doi.org/10.1007/s10021-005-0105-7.
- Cho, H.J., Kirui, P., Natarajan, H., 2008. Test of multi-spectral vegetation index for floating and canopy-forming submerged vegetation. Int. J. Environ. Res. Public Health 5, 477 483. https://doi.org/10.3390/ijerph5050477.
- Christensen, E.R., Nyholm, N., 1984. Ecotoxicological assays with algae: weibull doseresponse curves. Environ. Sci. Technol. 18, 713 718.
- Cleland, E.E., Chuine, I., Menzel, A., Mooney, H.A., Schwartz, M.D., 2007. Shifting plant phenology in response to global change. Trends Ecol. Evol. 22, 357 365. https://doi. org/10.1016/j.tree.2007.04.003.
- Cowling, S.A., Field, C.B., 2003. Environmental control of leaf area production: implications for vegetation and land-surface modeling. Glob. Biogeochem. Cycles 17. https://doi.org/10.1029/2002GB001915, 7 1-7 14.
- Crosby, S.C., Sax, D.F., Palmer, M.E., Booth, H.S., Deegan, L.A., Bertness, M.D., Leslie, H. M., 2016. Salt marsh persistence is threatened by predicted sea-level rise. Estuar. Coast. Shelf Sci. 181, 93–99. https://doi.org/10.1016/j.ecss.2016.08.018.
- Crotty, S.M., Ortals, C., Pettengill, T.M., Shi, L., Olabarrieta, M., Joyce, M.A., Altieri, A. H., Morrison, E., Bianchi, T.S., Craft, C., Bertness, M.D., Angelini, C., 2020. Sea-level rise and the emergence of a keystone grazer alter the geomorphic evolution and ecology of southeast US salt marshes. Proc. Natl. Acad. Sci. 201917869 https://doi.org/10.1073/pnas.1917869117.
- Dechant, B., Ryu, Y., Badgley, G., Köhler, P., Rascher, U., Migliavacca, M., Zhang, Y., Tagliabue, G., Guan, K., Rossini, M., Goulas, Y., Zeng, Y., Frankenberg, C., Berry, J. A., 2022. NIRVP: a robust structural proxy for sun-induced chlorophyll fluorescence and photosynthesis across scales. Remote Sens. Environ. 268, 112763 https://doi.org/10.1016/j.rse.2021.112763.
- Deegan, L.A., Johnson, D.S., Warren, R.S., Peterson, B.J., Fleeger, J.W., Fagherazzi, S., Wollheim, W.M., 2012. Coastal eutrophication as a driver of salt marsh loss. Nature 490, 388 392. https://doi.org/10.1038/nature11533.
- Feagin, R.A., Forbrich, I., Huff, T.P., Barr, J.G., Ruiz-Plancarte, J., Fuentes, J.D., Najjar, R.G., Vargas, R., Vázquez-Lule, A.L., Windham-Myers, L., Kroeger, K.D., Ward, E.J., Moore, G.W., Leclerc, M., Krauss, K.W., Stagg, C.L., Alber, M., Knox, S.H.,

- Schäfer, K.V.R., Bianchi, T.S., Hutchings, J.A., Nahrawi, H., Noormets, A., Mitra, B., Jaimes, A., Hinson, A.L., Bergamaschi, B., King, J.S., 2020. Tidal wetland gross primary production across the continental United States, 2000 2019. Glob. Biogeochem. Cycles. https://doi.org/10.1029/2019GB006349.
- Forbrich, I., Giblin, A.E., 2015. Marsh-atmosphere CO 2 exchange in a New England salt marsh. J. Geophys. Res. Biogeosci. 120, 1825 1838. https://doi.org/10.1002/ 2015/G003044
- Ge, Z.-M., Guo, H.-Q., Zhao, B., Zhang, C., Peltola, H., Zhang, L.-Q., 2016. Spatiotemporal patterns of the gross primary production in the salt marshes with rapid community change: a coupled modeling approach. Ecol. Model. 321, 110 120. https://doi.org/10.1016/j.ecolmodel.2015.11.003.
- Ghosh, S., Mishra, D.R., Gitelson, A.A., 2016. Long-term monitoring of biophysical characteristics of tidal wetlands in the northern Gulf of Mexico a methodological approach using MODIS. Remote Sens. Environ. 173, 39 58. https://doi.org/10.1016/j.rse.2015.11.015.
- Global Modeling and Assimilation Office (GMAO), 2015. MERRA-2 tavg1\_2d\_slv\_Nx: 2d,1-Hourly,Time-Averaged,Single-Level,Assimilation,Single-Level Diagnostics V5.12.4. NASA Goddard Earth Sci. Data Inf. Serv. Cent. GES DISC. https://doi.org/ 10.5067/VJAPPLI1CSIV.
- Gorelick, N., Hancher, M., Dixon, M., Ilyushchenko, S., Thau, D., Moore, R., 2017. Google Earth Engine: Planetary-scale geospatial analysis for everyone. Remote Sensing of Environment, Big Remotely Sensed Data: tools. Appl. Exp. 202, 18 27. https://doi.org/10.1016/j.rse.2017.06.031.
- Gorham, E., 1979. Shoot height, weight and standing crop in relation to density of monospecific plant stands. Nature 279, 148 150. https://doi.org/10.1038/ 279148a0
- Guo, H., Noormets, A., Zhao, B., Chen, Jiquan, Sun, G., Gu, Y., Li, B., Chen, Jiakuan, 2009. Tidal effects on net ecosystem exchange of carbon in an estuarine wetland. Agric. For. Meteorol., Special Section on Water and Carbon Dynamics in Selected Ecosystems in China 149, 1820 1828. https://doi.org/10.1016/j.agrformet.2009.06.010.
- Hawman, P.A., Mishra, D.R., O Connell, J.L., Cotten, D.L., Narron, C.R., Mao, L., 2021. Salt marsh light use efficiency is driven by environmental gradients and species-specific physiology and morphology. J. Geophys. Res. Biogeosci. 126 https://doi.org/10.1029/2020JG006213.
- Hladik, C., Alber, M., 2012. Accuracy assessment and correction of a LIDAR-derived salt marsh digital elevation model. Remote Sens. Environ. 121, 224 235. https://doi. org/10.1016/j.rse.2012.01.018.
- Hladik, C.M., Schalles, J., Alber, M., 2013. Salt marsh elevation and habitat mapping using hyperspectral and LIDAR data. Remote Sens. Environ. 139, 318–330. https://doi.org/10.1016/j.rse.2013.08.003.
- Hu, Q., Li, T., Deng, X., Wu, T., Zhai, P., Huang, D., Fan, X., Zhu, Y., Lin, Y., Xiao, X., Chen, X., Zhao, X., Wang, L., Qin, Z., 2022. Intercomparison of global terrestrial carbon fluxes estimated by MODIS and Earth system models. Sci. Total Environ. 810, 152231 https://doi.org/10.1016/j.scitotenv.2021.152231.
- Huete, A., Didan, K., Miura, T., Rodriguez, E.P., Gao, X., Ferreira, L.G., 2002. Overview of the radiometric and biophysical performance of the MODIS vegetation indices. Remote Sens. Environ. 83, 195 213. https://doi.org/10.1016/S0034-4257(02) 00096-2.
- Hughes, Z.J., FitzGerald, D.M., Wilson, C.A., Pennings, S.C., Więski, K., Mahadevan, A., 2009. Rapid headward erosion of marsh creeks in response to relative sea level rise. Geophys. Res. Lett. 36 https://doi.org/10.1029/2008GL036000.
- IPCC, 2019. In: Pörtner, H.-O., Roberts, D.C., Masson-Delmotte, V., Zhai, P., Tignor, M., Poloczanska, E., Mintenbeck, K., Alegría, A., Nicolai, M., Okem, A., Petzold, J., Rama, B., Weyer, N.M. (Eds.), The Ocean and Cryosphere in a Changing Climate: Special Report of the Intergovernmental Panel on Climate Change, 1st ed. Cambridge University Press. https://doi.org/10.1017/9781009157964.
- Jarvis, P.G., McNaughton, K.G., 1986. Stomatal control of transpiration: scaling up from leaf to region. In: Advances in Ecological Research. Elsevier, pp. 1 49. https://doi. org/10.1016/S0065-2504(08)60119-1.
- Kang, X., Yan, L., Zhang, X., Li, Y., Tian, D., Peng, C., Wu, H., Wang, J., Zhong, L., 2018. Modeling gross primary production of a typical coastal wetland in China using MODIS time series and CO2 Eddy flux tower data. Remote Sens. 10, 708. https://doi. org/10.3390/rs10050708.
- Kathilankal, J.C., Mozdzer, T.J., Fuentes, J.D., D Odorico, P., McGlathery, K.J., Zieman, J.C., 2008. Tidal influences on carbon assimilation by a salt marsh. Environ. Res. Lett. 3, 044010 https://doi.org/10.1088/1748-9326/3/4/044010.
- Kearney, M.S., Stutzer, D., Turpie, K., Stevenson, J.C., 2009. The effects of tidal inundation on the reflectance characteristics of coastal marsh vegetation. J. Coast. Res. 1177 1186 https://doi.org/10.2112/08-1080.1.
- Kirwan, M.L., Walters, D.C., Reay, W.G., Carr, J.A., 2016. Sea level driven marsh expansion in a coupled model of marsh erosion and migration: sea level driven marsh expansion. Geophys. Res. Lett. 43, 4366 4373. https://doi.org/10.1002/ 2016GL068507
- Kljun, N., Calanca, P., Rotach, M.W., Schmid, H.P., 2015. A simple two-dimensional parameterisation for flux footprint prediction (FFP). Geosci. Model Dev. 8, 3695–3713. https://doi.org/10.5194/gmd-8-3695-2015.
- Knox, S.H., Windham-Myers, L., Anderson, F., Sturtevant, C., Bergamaschi, B., 2018. Direct and indirect effects of tides on ecosystem-scale CO2 exchange in a brackish tidal marsh in northern California. J. Geophys. Res. Biogeosci. 123, 787 806. https://doi.org/10.1002/2017JG004048.
- Knyazikhin, Y., Martonchik, J.V., Myneni, R.B., Diner, D.J., Running, S.W., 1998.
  Synergistic algorithm for estimating vegetation canopy leaf area index and fraction of absorbed photosynthetically active radiation from MODIS and MISR data.
  J. Geophys. Res. Atmos. 103, 32257 32275. https://doi.org/10.1029/98JD02462.

- Kuhn, M., Wickham, H., 2020. Tidymodels: a collection of packages for modeling and machine learning using tidyverse principles. (manual).
- Langston, A.K., Alexander, C.R., Alber, M., Kirwan, M.L., 2021. Beyond 2100: elevation capital disguises salt marsh vulnerability to sea-level rise in Georgia, USA. Estuar. Coast. Shelf Sci. 249, 107093 https://doi.org/10.1016/j.ecss.2020.107093.
- Langston, A.K., Durán Vinent, O., Herbert, E.R., Kirwan, M.L., 2020. Modeling long-term salt marsh response to sea level rise in the sediment-deficient Plum Island estuary, MA. Limnol. Oceanogr. 65, 2142 2157. https://doi.org/10.1002/lno.11444.
- Liu, W., Pennings, S.C., 2019. Self-thinning and size-dependent flowering of the grass Spartina alterniflora across space and time. Funct. Ecol. 33, 1830 1841. https://doi. org/10.1111/1365-2435.13384.
- Lloyd, J., Taylor, J.A., 1994. On the temperature dependence of soil respiration. Funct. Ecol. 8, 315 323. https://doi.org/10.2307/2389824.
- Mariotti, G., 2020. Beyond marsh drowning: the many faces of marsh loss (and gain). Adv. Water Resour. 144, 103710 https://doi.org/10.1016/j. advwatres.2020.103710.
- Mauder, M., Foken, T., 2006. Impact of post-field data processing on eddy covariance flux estimates and energy balance closure. Meteorol. Z. 15, 597 609. https://doi. org/10.1127/0941-2948/2006/0167.
- Mendelssohn, I.A., Morris, J.T., 2002. Eco-physiological controls on the productivity of spartina alterniflora loisel. In: Weinstein, M.P., Kreeger, D.A. (Eds.), Concepts and Controversies in Tidal Marsh Ecology. Kluwer Academic Publishers, Dordrecht, pp. 59 80. https://doi.org/10.1007/0-306-47534-0 5.
- Mishra, D.R., Ghosh, S., 2015. Using moderate-resolution satellite sensors for monitoring the biophysical parameters and phenology of tidal marshes. In: Remote Sensing of Wetlands: Applications and Advances. CRC Press, Boca Raton FL, USA, pp. 300–331.
- Moffett, K.B., Wolf, A., Berry, J.A., Gorelick, S.M., 2010. Salt marsh atmosphere exchange of energy, water vapor, and carbon dioxide: effects of tidal flooding and biophysical controls. Water Resour. Res. 46 https://doi.org/10.1029/ 2009WR009041.
- Moncrieff, J., Clement, R., Finnigan, J., Meyers, T., 2005. Averaging, detrending, and filtering of Eddy covariance time series. In: Lee, X., Massman, W., Law, B. (Eds.), Handbook of Micrometeorology. Kluwer Academic Publishers, Dordrecht, pp. 7–31. https://doi.org/10.1007/1-4020-2265-4-2.
- Moncrieff, J., Massheder, J.M., de Bruin, H., Elbers, J., Friborg, T., Heusinkveld, B., Kabat, P., Scott, S., Soegaard, H., Verhoef, A., 1997. A system to measure surface fluxes of momentum, sensible heat, water vapour and carbon dioxide. J. Hydrol. 188 189, 589 611. https://doi.org/10.1016/S0022-1694(96)03194-0.
- Myneni, R., Knyazikhin, Y., Park, T., 2015. MYD15A2H MODIS/Aqua Leaf Area Index/FPAR 8-Day L4 Global 500m SIN Grid V006. https://doi.org/10.5067/MODIS/MYD15A9H 006
- Nahrawi, H., Leclerc, M.Y., Pennings, S., Zhang, G., Singh, N., Pahari, R., 2020. Impact of tidal inundation on the net ecosystem exchange in daytime conditions in a salt marsh. Agric. For. Meteorol. 294, 108133 https://doi.org/10.1016/j. agrformet.2020.108133.
- Najjar, R.G., Herrmann, M., Alexander, R., Boyer, E.W., Burdige, D.J., Butman, D., Cai, W.-J., Canuel, E.A., Chen, R.F., Friedrichs, M.A.M., Feagin, R.A., Griffith, P.C., Hinson, A.L., Holmquist, J.R., Hu, X., Kemp, W.M., Kroeger, K.D., Mannino, A., McCallister, S.L., McGillis, W.R., Mulholland, M.R., Pilskaln, C.H., Salisbury, J., Signorini, S.R., St-Laurent, P., Tian, H., Tzortziou, M., Vlahos, P., Wang, Z.A., Zimmerman, R.C., 2018. Carbon budget of tidal wetlands, estuaries, and shelf waters of eastern North America. Glob. Biogeochem. Cycles 32, 389 416. https://doi.org/10.1002/2017/6B005790.
- Narron, C.R., O Connell, J.L., Mishra, D.R., Cotten, D.L., Hawman, P.A., Mao, L., 2022. Flooding in Landsat across tidal systems (FLATS): an index for intermittent tidal filtering and frequency detection in salt marsh environments. Ecol. Indic. 141, 109045 https://doi.org/10.1016/j.ecolind.2022.109045.
- Nellemann, C., Corcoran, E., 2009. Blue carbon: the role of healthy oceans in binding carbon: a rapid response assessment.UNEP/Earthprint.
- Nobel, P.S., 1983. Biophysical Plant Physiology and Ecology. W.H Freeman, San Francisco
- O Connell, J.L., Mishra, D.R., Cotten, D.L., Wang, L., Alber, M., 2017. The Tidal Marsh Inundation Index (TMII): an inundation filter to flag flooded pixels and improve MODIS tidal marsh vegetation time-series analysis. Remote Sens. Environ. 201, 34 46. https://doi.org/10.1016/j.rse.2017.08.008.
- Papale, D., Reichstein, M., Aubinet, M., Canfora, E., Bernhofer, C., Kutsch, W., Longdoz, B., Rambal, S., Valentini, R., Vesala, T., Yakir, D., 2006. Towards a standardized processing of net ecosystem exchange measured with eddy covariance technique: algorithms and uncertainty estimation. Biogeosciences 3, 571 583. https://doi.org/10.5194/bg-3-571-2006.
- Park, H., Jeong, S., 2021. Leaf area index in earth system models: how the key variable of vegetation seasonality works in climate projections. Environ. Res. Lett. 16, 034027 https://doi.org/10.1088/1748-9326/abe2cf.
- Pennings, S.C., Georgia Coastal Ecosystems LTER Project, 2022. Monthly vegetation and invertebrate population monitoring near the Georgia coastal ecosystems LTER flux tower ver 83. Environmental Data Initiative. https://doi.org/10.6073/pasta/7f0 6441e8c200b6429dee520a3cc3366.
- Pennings, S.C., Grant, M.-B., Bertness, M.D., 2005. Plant zonation in low-latitude salt marshes: disentangling the roles of flooding, salinity and competition. J. Ecol. 93, 159 167. https://doi.org/10.1111/j.1365-2745.2004.00959.x.
- Pezeshki, S.R., 1997. Photosynthesis and root growth in Spartina alterniflora in relation to root zone aeration. Photosynthetica 34, 107 114. https://doi.org/10.1023/A: 1006820019220.
- R Core Team, 2020. R: A Language and Environment for Statistical Computing. R Foundation for Statistical Computing, Vienna, Austria.

- Ramsey III, E., Nelson, G., Baarnes, F., Spell, R., 2004. Light attenuation profiling as an indicator of structural changes in coastal marshes. In: Lunetta, R.S., Lyon, J.G. (Eds.), Remote Sensing and GIS Accuracy Assessment. CRC, New York, NY, pp. 59–73.
- Reidenbaugh, T.G., Banta, W.C., 1980. Origins and effects of spartina wrack in a Virginia salt marsh. Gulf Res. Rep. 6 https://doi.org/10.18785/grr.0604.07.
- Ritz, C., Baty, F., Streibig, J.C., Gerhard, D., 2015. Dose-response analysis using r. PLOS
- Running, S.W., Baldocchi, D.D., Turner, D.P., Gower, S.T., Bakwin, P.S., Hibbard, K.A., 1999. A global terrestrial monitoring network integrating tower fluxes, flask sampling, ecosystem modeling and EOS satellite data. Remote Sens. Environ. 70, 108 127. https://doi.org/10.1016/S0034-4257(99)00061-9.
- Running, S.W., Hunt, E.R., 1993. Generalization of a Forest ecosystem process model for other biomes, BIOME-BGC, and an application for global-scale models. In: Ehleringer, J.R., Field, C.B. (Eds.), Scaling Physiological Processes, Physiological Ecology. Academic Press, San Diego, pp. 141 158. https://doi.org/10.1016/B978-0-12-233440-5.50014-2.
- Running, S.W., Nemani, R.R., Heinsch, F.A., Zhao, M., Reeves, M., Hashimoto, H., 2004. A continuous satellite-derived measure of global terrestrial primary production. Bioscience 54, 547 560. https://doi.org/10.1641/0006-3568(2004)054[0547: ACSMOGI2 0.0022
- Running, S.W., Zhao, M., 2015. User s Guide: Daily GPP and Annual NPP MOD17A2/A3)
  Products: NASA Earth observing System MODIS Land Algorithm.
- Schuerch, M., Spencer, T., Temmerman, S., Kirwan, M.L., Wolff, C., Lincke, D., McOwen, C.J., Pickering, M.D., Reef, R., Vafeidis, A.T., Hinkel, J., Nicholls, R.J., Brown, S., 2018. Future response of global coastal wetlands to sea-level rise. Nature 561, 231 234. https://doi.org/10.1038/s41586-018-0476-5.
- Smith, S.M., Lee, K.D., 2015. The influence of prolonged flooding on the growth of Spartina alterniflora in Cape Cod (Massachusetts, USA). Aquat. Bot. 127, 53 56. https://doi.org/10.1016/j.aquabot.2015.08.002.
- Sun, C., Li, J., Liu, Yongxue, Liu, Yongchao, Liu, R., 2021. Plant species classification in salt marshes using phenological parameters derived from Sentinel-2 pixeldifferential time-series. Remote Sens. Environ. 256, 112320 https://doi.org/ 10.1016/j.rse.2021.112320.
- Tao, J., Mishra, D.R., Cotten, D.L., O Connell, J., Leclerc, M., Nahrawi, H.B., Zhang, G., Pahari, R., 2018. A comparison between the MODIS product (MODI7A2) and a tiderobust empirical GPP model evaluated in a Georgia wetland. Remote Sens. 10, 1831. https://doi.org/10.3390/rs10111831.
- Teske, M.E., Thistle, H.W., 2004. A library of forest canopy structure for use in interception modeling. For. Ecol. Manag. 198, 341 350. https://doi.org/10.1016/j. foreco.2004.05.031.
- Troxler, T.G., Gaiser, E., Barr, J., Fuentes, J.D., Jaffe, R., Childers, D.L., Collado-Vides, L., Rivera-Monroy, V.H., Castaneda-Moya, E., Anderson, W., et al., 2013. Integrated carbon budget models for the Everglades terrestrial-coastal-oceanic gradient: current status and needs for inter-site comparisons. Oceanography 26, 98 107.
- Vickers, D., Mahrt, L., 1997. Quality control and flux sampling problems for tower and aircraft data. J. Atmos. Ocean. Technol. 14, 512 526. https://doi.org/10.1175/ 1520-0426(1997)014 0512:OCAFSP 2.0.CO:2.

- Vitousek, S., Barnard, P.L., Fletcher, C.H., Frazer, N., Erikson, L., Storlazzi, C.D., 2017. Doubling of coastal flooding frequency within decades due to sea-level rise. Sci. Rep. 7, 1399. https://doi.org/10.1038/s41598-017-01362-7.
- Voss, C.M., Christian, R.R., Morris, J.T., 2013. Marsh macrophyte responses to inundation anticipate impacts of sea-level rise and indicate ongoing drowning of North Carolina marshes. Mar. Biol. 160, 181 194. https://doi.org/10.1007/s00227-012-2076-5
- Webb, E.K., Pearman, G.I., Leuning, R., 1980. Correction of flux measurements for density effects due to heat and water vapour transfer. Q. J. R. Meteorol. Soc. 106, 85 100. https://doi.org/10.1002/qj.49710644707.
- Weibull, W., 1951. A statistical distribution function of wide applicability. J. Appl. Mech. 18, 293 297. https://doi.org/10.1115/1.4010337.
- Wilczak, J.M., Oncley, S.P., Stage, S.A., 2001. Sonic anemometer tilt correction algorithms. Bound.-Layer Meteorol. 99, 127 150. https://doi.org/10.1023/A: 101106500465
- Wood, D.A., 2022. Net ecosystem exchange comparative analysis of the relative influence of recorded variables in well monitored ecosystems. Ecol. Complex. 50, 100998 https://doi.org/10.1016/j.ecocom.2022.100998.
- Wu, F., Pennings, S.C., Ortals, C., Ruiz, J., Farrell, W.R., McNichol, S.M., Angelini, C., Spivak, A.C., Alber, M., Tong, C., 2021. Disturbance is complicated: headwarderoding saltmarsh creeks produce multiple responses and recovery trajectories. Limnol. Oceanogr. https://doi.org/10.1002/lno.11867 n/a.
- Wu, M., Muhammad, S., Chen, F., Niu, Z., Wang, C., 2015. Combining remote sensing and eddy covariance data to monitor the gross primary production of an estuarine wetland ecosystem in East China. Environ. Sci. Process. Impacts 17, 753–762. https://doi.org/10.1039/C5EM00061K.
- Xie, X., Li, A., Jin, H., Tan, J., Wang, C., Lei, G., Zhang, Z., Bian, J., Nan, X., 2019. Assessment of five satellite-derived LAI datasets for GPP estimations through ecosystem models. Sci. Total Environ. 690, 1120 1130. https://doi.org/10.1016/j. scitotenv.2019.06.516.
- Yan, Y.-E., Guo, H.-Q., Gao, Y., Zhao, B., Chen, J.-Q., Li, B., Chen, J.-K., 2010. Variations of net ecosystem CO 2 exchange in a tidal inundated wetland: coupling MODIS and tower-based fluxes. J. Geophys. Res. 115 https://doi.org/10.1029/2009JD012838.
- Yan, Y.-E., Zhao, B., Chen, J., Guo, H., Gu, Y., Wu, Q., Li, B., 2008. Closing the carbon budget of estuarine wetlands with tower-based measurements and MODIS time series. Glob. Change Biol. 14, 1690 1702. https://doi.org/10.1111/j.1365-2486.2008.01589.x.
- Yang, X., Miller, D.R., Montgomery, M.E., 1993. Vertical distributions of canopy foliage and biologically active radiation in a defoliated/refoliated hardwood forest. Agric. For. Meteorol. 67, 129 146. https://doi.org/10.1016/0168-1923(93)90054-L.
- Yu, J., Wang, Y., Li, Y., Dong, H., Zhou, D., Han, G., Wu, H., Wang, G., Mao, P., Gao, Y., 2012. Soil organic carbon storage changes in coastal wetlands of the modern Yellow River Delta from 2000 to 2009. Biogeosciences 9, 2325–2331. https://doi.org/10.5194/bg-9-2325-2012.